ResearchGate

See discussions, stats, and author profiles for this publication at: http://www.researchgate.net/publication/258443416

A novel nickel-chelated surfactant for affinity-based aqueous two-phase micellar extraction of histidine-rich protein

ARTICLE *in* JOURNAL OF CHROMATOGRAPHY A · OCTOBER 2013

Impact Factor: 4.26 · DOI: 10.1016/j.chroma.2013.10.074 · Source: PubMed

CITATIONS
4

DOWNLOADS
33

VIEWS
82

4 AUTHORS, INCLUDING:

Shuo Wang

2 PUBLICATIONS **5** CITATIONS

SEE PROFILE

Neng Xiong

International University of Japan

2 PUBLICATIONS **5** CITATIONS

SEE PROFILE

Xiao Yan-Dong

91 PUBLICATIONS **907** CITATIONS

SEE PROFILE

Available from: Shuo Wang
Retrieved on: 21 September 2015

Journal of Chromatography A, 1320 (2013) 118–124

Contents lists available at ScienceDirect

Journal of Chromatography A

journal homepage: www.elsevier.com/locate/chroma

A novel nickel-chelated surfactant for affinity-based aqueous two-phase micellar extraction of histidine-rich protein

Shuo Wang [a], Neng Xiong [a], Xiao-Yan Dong [a,b], Yan Sun [a,b,*]

[a] Department of Biochemical Engineering and Key Laboratory of Systems Bioengineering of the Ministry of Education, School of Chemical Engineering and Technology, Tianjin University, Tianjin 300072, China
[b] Collaborative Innovation Center of Chemical Science and Engineering (Tianjin), Tianjin 300072, China

ARTICLE INFO

Article history:
Received 28 June 2013
Received in revised form
18 September 2013
Accepted 23 October 2013
Available online 30 October 2013

Keywords:
Aqueous two-phase micellar system
Nickel-chelated surfactant
Triton X-114
Cloud point
Affinity partitioning
Green fluorescent protein

ABSTRACT

Aqueous two-phase micellar systems (ATPMSs) composed of nonionic surfactants are considered promising for the separation and purification of proteins. To improve the specificity of ATPMSs, a novel nickel-chelated surfactant was prepared by successive modifications of Triton X-114 (TX). Characterizations by Fourier transformation infrared spectroscopy demonstrated the successful synthesis of the nickel-chelated surfactant (TX-Ni). The cloud point, critical micelle concentration (CMC), molecular interaction parameter and micelle size were measured for the mixed surfactant system of TX-Ni and TX to achieve a full understanding of their aggregation behaviors. The results showed that mixed micelles were formed, and the cloud point increased with the mole fraction of TX-Ni because TX-Ni had a more hydrophilic head group than TX. Moreover, the reduction of micelle size revealed by light scattering experiments indicated that the insertion of TX-Ni inhibited the micellar growth due to the increased steric and electrostatic repulsion. Finally, the efficiency of TX-Ni as an affinity surfactant was demonstrated by the affinity partitioning of histidine-tagged enhanced green fluorescent protein with an over 20-fold increase of the partition coefficient (from 0.60 to 12.42). This affinity-based ATPMS is thus considered promising for providing a versatile platform for the separation of histidine-rich proteins.

© 2013 Elsevier B.V. All rights reserved.

1. Introduction

Aqueous two-phase systems (ATPSs) are cost-effective and environment-friendly platforms for the separation of proteins. In recent years, ATPSs have attracted considerable interest and are regarded as an alternative to traditional separation techniques owing to their advantages, including scale-up potential, continuous operation, ease of process integration and biocompatibility [1–5]. Apart from conventional ATPSs which are composed of two incompatible polymers or one polymer and a salt [1], many new ATPSs have been developed, one of which is the aqueous two-phase micellar system (ATPMS) formed by nonionic surfactants [6]. When heated above a threshold temperature, which is known as cloud point, the homogenous aqueous solution of nonionic surfactant becomes turbid and then separates into two immiscible phases. Usually one phase is rich in micelles and the other is poor. Due to the different physicochemical properties of the two phases, proteins partition unevenly in this system [6]. Because both the micelle-rich phase and the micelle-poor phase are mainly composed of water and most nonionic surfactants are mild to proteins [7], ATPMSs provide a gentle and friendly environment for biomolecules. Compared with ATPSs composed of polymers, ATPMSs have some merits [8,9]: (1) micelles are labile entities formed by noncovalent binding of individual surfactant molecules, and as a result, the micelle shape and size are adjustable. (2) Generally, commercial nonionic surfactants are easily available and cheap. (3) More importantly, nonionic surfactants have been widely utilized in industries for a long time and the basic data are relatively abundant, which is beneficial for industrial applications.

ATPMSs were originally used for the concentration of zinc ions [10]. In the 1980s, Bordier investigated their application in the separation of membrane proteins [11]. Since then ATPMSs have been successfully applied to the extraction and purification of a variety of proteins and related biochemicals [6,12]. Particularly, ATPMSs are most suitable for the isolation of hydrophobic membrane proteins. In this case, the separation is governed by solubilization and hydrophobic effects, which determine the partitioning extent of proteins into the micelle-rich phase. Although the contributions of excluded-volume effects [13] and electrostatic interactions [14] have extended the applications of this method to the extraction of hydrophilic proteins, its low selectivity remains to be an obstacle

* Corresponding author at: Department of Biochemical Engineering and Key Laboratory of Systems Bioengineering of the Ministry of Education, School of Chemical Engineering and Technology, Tianjin University, Tianjin 300072, China.
Tel.: +86 22 27404981; fax: +86 22 27404981.
E-mail address: ysun@tju.edu.cn (Y. Sun).

0021-9673/$ – see front matter © 2013 Elsevier B.V. All rights reserved.
http://dx.doi.org/10.1016/j.chroma.2013.10.074

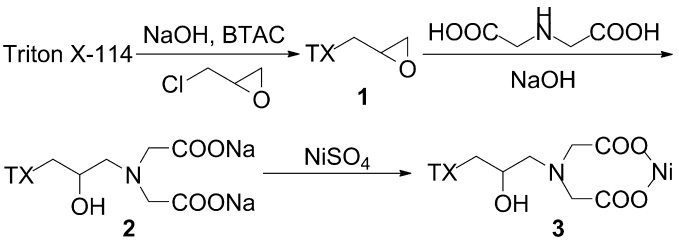

Fig. 1. Synthesis route for the nickel-chelated surfactant (TX-Ni).

precluding its wide utilizations. Generally, the use of affinity ligands is an effective way to improve the specificity of ATPMSs [3,15–20]. However, in spite of the fact that immobilized metal-ion affinity ligands have been successfully applied in polymer ATPS [21,22], reverse micelle extraction [23,24], as well as the most widely used immobilized metal affinity chromatography (IMAC) [25], there are no reports on their incorporation into ATPMSs.

In this study, Triton X-114 (TX) was functionalized by successive modifications of epichlorohydrin and iminodiacetic acid (IDA) followed by chelating with nickel ions to prepare a novel metal-chelated surfactant, TX-Ni. Then, an affinity-based ATPMS was formed by the mixture of TX-Ni and TX. The system was extensively characterized and the effectiveness of this affinity-based ATPMS was demonstrated by the affinity partitioning and separation of histidine-tagged enhanced green fluorescent protein (EGFP).

2. Materials and methods

2.1. Materials

TX was obtained from Fluka (Bucks, Switzerland). Acetonitrile (≥99.9%), pyrene (≥99.0%) and chicken egg white lysozyme (≥90%) were purchased from Sigma–Aldrich (MO, USA). IDA (>97%) and benzyltriethylammonium chloride (BTAC, >99%) were from Guangfu (Tianjin, China). Other chemicals were all of analytical grade from local sources. All materials were used as received.

Polyhistidine-tagged EGFP was expressed by cultivation of the recombinant *Escherichia coli* harboring the vector pET28a-EGFP as described previously [26]. The cells were harvested by centrifugation and disrupted by sonication in Tris–HCl buffer (20 mmol/L Tris, 100 mmol/L NaCl, pH 8.0). After centrifugation of the cell homogenate at 13,000 × *g* for 15 min at 4 °C, the supernatant was purified by IMAC and gel filtration chromatography to prepare pure EGFP [23].

2.2. Synthesis of nickel-chelated surfactant

The synthesis of TX-Ni was performed according to the procedures described in literatures [27,28] and the synthesis route is illustrated in Fig. 1. In a typical procedure, 5.4 g of TX (0.01 mol) was added to 10 mL of benzene with 1 g of NaOH and 0.5 g of BTAC. The mixture was vigorously stirred under N_2 at 50 °C for 30 min. Then, 4 mL of epichlorohydrin (0.05 mol) was added and the stirring was continued for 4 h. The reaction mixture was filtered to remove solids and excess organic solvents were removed by vacuum evaporation. This reaction led to the activation of TX to the intermediate epoxide (**1** in Fig. 1), which was obtained as yellow oil. In the following reaction, **1** was mixed with 20 mL of 2 mol/L disodium iminodiacetate solution (pH 11) prepared by slowly adding NaOH pellets to 6.6 g of IDA in water. The mixture was stirred at 50 °C for 24 h. Separation of the IDA coupled TX (TX-IDA, **2** in Fig. 1) was achieved by extraction with chloroform [17]. Thereafter, TX-IDA in the organic phase was recovered and dried by vacuum evaporation, and then mixed with 20 mL of 0.5 mol/L $NiSO_4$ solution to chelate Ni(II) ions. Separation of TX-Ni (**3** in Fig. 1) was the same as that of TX-IDA. Finally, the product was purified by redissolving in ethyl acetate and then reprecipitating with *n*-hexane. After suction filtration, residue organic solvents were removed by drying under vacuum at 80 °C overnight.

2.3. Characterization of TX and TX-Ni

Fourier transform infrared (FTIR) analysis was performed on a Tensor 27 FTIR spectrometer (Bruker Optics, Billerica, MA). Potassium bromide (KBr) was used to collect the background. Samples were mixed with KBr in an appropriate portion before spectrum collection. Twenty scans were recorded at 4 cm^{-1} resolution with two levels of zero filling.

The purity of TX-Ni was determined by reversed-phase high performance liquid chromatography (RP-HPLC) using a C18 Symmetry® column (5 μm, 150 mm × 4.6 mm; Waters, MA, USA). Samples were eluted with a 20:80 water–acetonitrile mobile phase containing 0.1% trifluoroacetic acid at 0.5 mL/min [29]. The analysis was performed on an Agilent 1100 system (Agilent Technologies, USA) equipped with a UV detector set at 277 nm.

2.4. Phase diagram determination

Phase diagrams for the aqueous solutions of TX-Ni and TX were measured by the cloud-point method [13]. Briefly, surfactant solutions of known concentrations were prepared and then put into a programmable temperature controller (PolyScience 9512, PolyScience, USA) with a temperature stability of ±0.01 °C (readout accuracy: ±0.25 °C). At beginning, each sample was cooled to 20 °C which was low enough to make the solution exhibit a single and clear phase. The temperature was then raised at 0.2 °C/min until the solution became turbid, indicating the onset of phase separation, at a temperature T_u. As soon as clouding was observed, the temperature was lowered at 0.2 °C/min until the solution became clear again at a temperature T_d. The cloud point temperature was taken to be the average of T_u and T_d. The procedure was repeated three times for each data point to ensure reproducibility.

2.5. Determination of critical micelle concentration

The critical micelle concentrations (CMCs) of TX-Ni, TX and their mixtures were determined by the pyrene 1:3 ratio method [30]. A number of surfactant solutions containing 2 μmol/L of pyrene were measured on a Perkin Elmer LS55 Fluorescence Spectrometer (Waltham, MA, USA). Pyrene was excited at 335 nm. The emission intensities of the peaks located near 373 nm (I_1) and 384 nm (I_3) were recorded. The solution composition was expressed by the mole fraction of TX-Ni (α), defined as:

$$\alpha = \frac{[\text{TX-Ni}]}{[\text{TX-Ni}] + [\text{TX}]} \quad (1)$$

where [TX-Ni] and [TX] are the molar concentrations of TX-Ni and TX in the solution, respectively. All measurements were carried out at 20.0 ± 0.1 °C.

2.6. Light scattering

Static light scattering (SLS) experiments were performed with a DAWN EOS multiangle light scattering instrument (Wyatt Technology, USA). All measurements were conducted in the angular range $30° < \theta < 150°$ at a wavelength of $\lambda = 690$ nm. The

apparent weight-average molecular weight (M_{app}) of micelles was calculated with the Zimm equation [31]:

$$\frac{Kc}{\Delta R_\theta(q)} \approx \frac{1}{M_{app}P(q)} + 2A_2c \quad (2)$$

Here, $K = 4\pi^2 n_0^2 (dn/dc)^2/\lambda_0^4 N_A$ is the scattering constant, $q = ((4\pi n)/\lambda_0)\sin(\theta/2)$ is the scattering vector, c is the micelle concentration, $\Delta R_\theta(q)$ is the excess Rayleigh ratio, $P(q)$ is the particle scattering factor, and A_2 is the second virial coefficient (n_0, the refractive index of water; dn/dc, the refractive index increment; λ_0, the wavelength of light in vacuum; N_A, Avogadro's number). The refractive index increment was measured with an Optilab DSP interferometric refractometer (Wyatt Technology, Santa Barbara, CA).

Dynamic light scattering (DLS) measurements were carried out on a Zetasizer Nano ZS (Malvern, UK) equipped with a 633 nm He–Ne laser. Scattered light was detected at the fixed angle of 173°. The apparent hydrodynamic diameter (D_H) was obtained *via* the Stokes–Einstein equation:

$$D_H = \frac{k_B T}{3\pi\eta D_{app}} \quad (3)$$

where k_B is the Boltzmann constant, T is the absolute temperature, η is the viscosity of water and D_{app} is the apparent diffusion coefficient.

Surfactant solutions for light scattering experiments were filtered through 0.22 μm membranes to remove particulate materials. All measurements were performed at 20.0 ± 0.1 °C.

2.7. Protein partitioning experiments

All samples for the partitioning experiment were prepared at pH 8.0 using Tris–HCl buffer solutions (20 mmol/L Tris, 100 mmol/L NaCl). Equal volumes (1.5 mL) of 0.08 g/mL surfactant solution and 0.2 mg/mL protein solution were mixed and equilibrated at 4 °C to exhibit a clear and homogeneous phase. Then, the samples were placed in a water bath to undergo phase separation. The operating temperature was set at the cloud point of the surfactant solution. When the partitioning equilibrium was reached after 2 h, the two coexisting phases were separated carefully.

EGFP concentration in each phase was determined by fluorometric assay with excitation and emission wavenumbers of 488 nm and 509 nm, respectively [26]. The concentration of lysozyme was measured by RP-HPLC on an Agilent 1100 system using a ZORBAX Eclipse XDB-C8 column (4.6 mm × 150 mm; Agilent Technologies, USA). The mobile phase consisted of a gradient of water and acetonitrile both containing 0.1% trifluoroacetic acid was run at a flow rate of 1 mL/min. After a 5-min equilibration period at 70% water, a linear gradient from 70% to 50% water in 25 min was implemented. Detection was carried out with a UV detector at 215 nm.

The partitioning behavior of proteins was quantitatively studied in terms of the partition coefficient K_P, defined as:

$$K_P = \frac{[P]_r}{[P]_p} \quad (4)$$

where $[P]_r$ and $[P]_p$ are the protein concentrations in the micelle-rich and the micelle-poor phases, respectively.

The volume ratio (V_R) between the two phases was calculated as:

$$V_R = \frac{V_r}{V_p} \quad (5)$$

where V_r and V_p are the volumes of micelle-rich and micelle-poor phases, respectively.

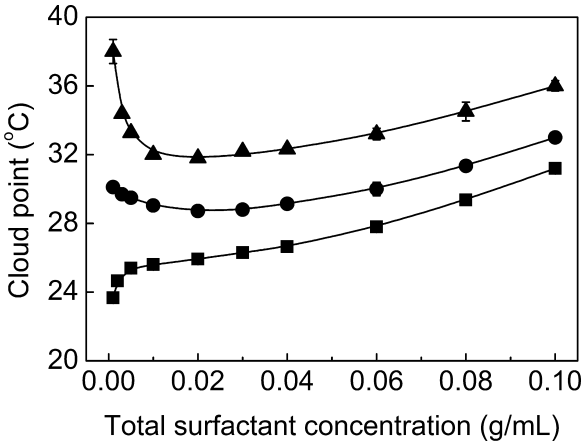

Fig. 2. Coexistence curves for the surfactant/water systems at different mole fractions of TX-Ni (α): (■) $\alpha = 0$, (●) $\alpha = 0.05$ and (▲) $\alpha = 0.1$. The solid lines are drawn for guiding the eyes.

The extraction yield (E) was calculated according to the following equation:

$$E = \frac{[P]_r V_r}{[P]_i V_i} \times 100\% \quad (6)$$

where $[P]_i$ and V_i are the initial protein concentration and solution volume prior to phase separation, respectively.

The separation factor (S) was calculated as:

$$S = \frac{K_{EGFP}}{K_{LYZ}} \quad (7)$$

where K_{EGFP} and K_{LYZ} are the partition coefficients of EGFP and lysozyme, respectively.

Triplicate partitioning or separation experiments were performed and the average values with standard deviations were presented.

3. Results and discussion

3.1. Characterization of the nickel-chelated surfactant

TX was converted into a nickel-chelated surfactant *via* the coupling of IDA. The successful synthesis of TX-Ni was confirmed by FTIR (Fig. S1 in Supplementary Material). According to the literature [32], the strong absorption at 1588 cm^{-1} was attributed to the asymmetric stretch of the nickel-complexed carboxylate group while the uncomplexed symmetric carboxylate peak appeared at 1410 cm^{-1}. The peak at 1727 cm^{-1} was assigned to the protonated carboxylic acid groups. The yield of TX-Ni was 55.1% with a purity of 95.3% determined by HPLC.

The retention time of TX-Ni was shorter than TX (Fig. S2 in Supplementary Material), indicating that the Ni(II)-IDA moiety increased the hydrophilicity of TX. Taking into account that TX is a mixture of polyoxyethylene ethers, the product was not further purified and its properties were considered as average ones.

3.2. Phase diagram

Aqueous solutions of nonionic surfactants will become turbid when heated above the cloud point. This phenomenon is attributed to the efficient dehydration of the hydrophilic portion of micelles at higher temperature, which increases the attractive interactions among micelles and thus facilitates the formation of large aggregates [33]. It can be seen from Fig. 2 that the cloud point increased with the mole fraction of TX-Ni. Besides, no phase separation was observed for TX-Ni even if its solution was heated to boiling. These

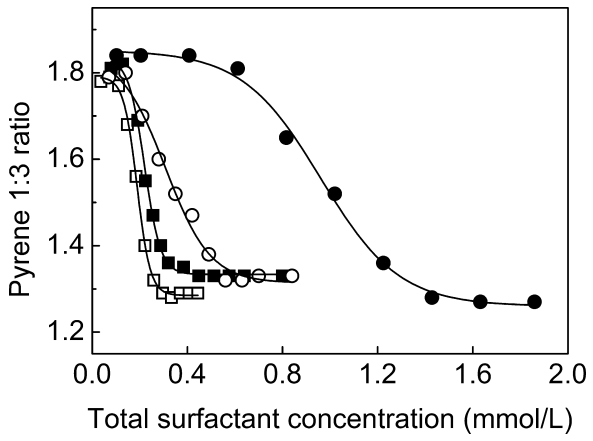

Fig. 3. Plots of pyrene 1:3 ratio *versus* total surfactant concentration of TX and TX-Ni mixtures at some typical mole fractions of TX-Ni (α): (□) $\alpha = 0$, (■) $\alpha = 0.4$, (○) $\alpha = 0.8$ and (●) $\alpha = 1.0$.

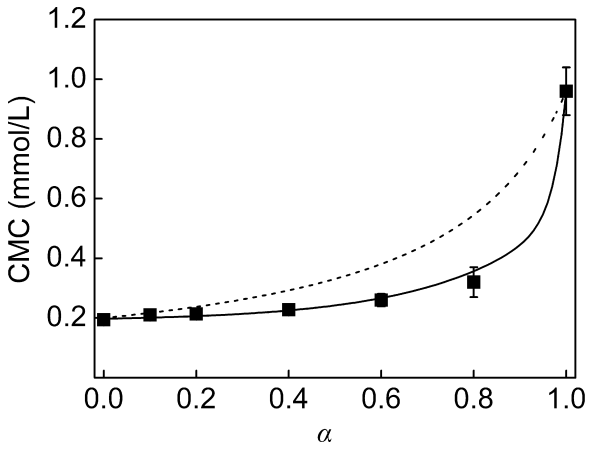

Fig. 4. Experimental (■) and predicted (lines) critical micelle concentrations of TX-Ni/TX mixtures as a function of the mole fraction of TX-Ni (α). The dashed line represents ideal mixing calculated from Eqs. (8) to (10) with $\beta = 0$, whereas the solid line is the predicted CMCs with $\beta = -1.7$.

results were ascribed to the increased hydrophilicity of micelles offered by the Ni(II)-IDA moiety, which made the dehydration difficult [34]. In addition, the polarization of TX-Ni might also play a role as the cloud point of TX was dramatically increased with even small amounts of ionic surfactants [35]. It is worth noting that the increase of cloud point is not favorable for dealing with biomolecules. Hence, only the mixtures with relatively low cloud points were investigated.

It is well known that the formation of micelles is governed by the tendency of hydrophobic chains to minimize contact with water. As this tendency is balanced by the hydration and the space required by the polar heads of nonionic surfactants, the insertion of TX-Ni which had a larger and more hydrophilic polar head was expected to inhibit the formation of large micelles [36]. The micellization process was further studied in the following sections.

3.3. Molecular interactions between TX and TX-Ni

The CMC values of surfactant mixtures were measured and analyzed by the regular solution theory. For the calculation of fitting curves, the mass concentration was converted to molar concentration using molecular weights of 744 g/mol and 537 g/mol for TX-Ni and TX, respectively. Fig. 3 presents the pyrene 1:3 ratio (I_1/I_3) plots as a function of surfactant concentration as well as the mole fraction of TX-Ni. Following Aguiar et al. [30], the data were fitted by a Boltzmann-type sigmoid and the center of the sigmoid was selected as the CMC value. The CMC data at different mole fractions of TX-Ni are listed in Table 1 and the CMC of 0.20 mmol/L for TX is in good agreement with the literature data [37]. It is obvious that CMC increased with increasing TX-Ni, revealing that the presence of TX-Ni inhibited the formation of micelles. Additionally, the reduction in the slope of the sigmoidal curve around CMC suggested that the micellization process was unfavorable on the addition of TX-Ni [30].

The behavior of many mixed surfactant systems can be understood *via* the deviation from ideal mixing using the regular solution theory [38]. The magnitude of nonideality is expressed in terms of an interaction parameter (β). In spite of the fact that neither TX-Ni nor TX is homogeneous, this method can also be used for qualitative analysis and show possible trends [39].

Table 1
Critical micelle concentration (cmc_{12}), composition of the micelles (x_1) and interaction parameter (β) at different mole fractions of TX-Ni (α).

α	0	0.1	0.2	0.4	0.6	0.8	1.0
cmc_{12} (mmol/L)	0.20	0.21	0.21	0.23	0.26	0.32	0.96
x_1	–	0.05	0.13	0.24	0.35	0.48	–
β	–	−0.9	−1.4	−1.6	−1.8	−2.2	–

According to the regular solution theory [38], the CMC of a surfactant mixture can be expressed as:

$$\frac{1}{cmc_{12}} = \frac{\alpha}{f_1 cmc_1} + \frac{1-\alpha}{f_2 cmc_2} \tag{8}$$

where cmc_1, cmc_2 and cmc_{12} are the CMCs of TX-Ni, TX and their mixture, respectively. The activity coefficients of TX-Ni and TX (f_1 and f_2, respectively) are given by $f_1 = \exp[\beta(1-x_1)^2]$ and $f_2 = \exp(\beta x_1{}^2)$. The variable x_1 is the mole fraction of TX-Ni in the micelles. The interaction parameter β not only accounts for the deviation from ideality but also indicates the degree of intramicellar interactions. In general, a more negative β value indicates a more attractive interaction between two different surfactant molecules and demixing will occur for $\beta > 2$ [40,41]. When the CMC of the mixture is known, x_1 can be solved iteratively from:

$$\frac{x_1^2 \ln(\alpha cmc_{12}/x_1 cmc_1)}{(1-x_1)^2 \ln((1-\alpha)cmc_{12}/(1-x_1)cmc_2)} = 1 \tag{9}$$

and β can be evaluated from:

$$\beta = \frac{\ln(\alpha cmc_{12}/x_1 cmc_1)}{(1-x_1)^2} \tag{10}$$

The dependence of cmc_{12} on the mole fraction of TX-Ni is shown in Fig. 4. The solid line represents the predicted CMCs with $\beta = -1.7$. The negative deviation from ideal mixing implied the formation of mixed micelles and the negative values of β (Table 1) revealed the attractive interactions between TX-Ni and TX. This could be attributed to the fact that the presence of TX screened the steric and electrostatic repulsion between the polar head of TX-Ni [42,43].

3.4. Effect of TX-Ni on micellar growth

Fig. 5 shows the concentration dependence of the apparent molecular weight of the micelles. To describe the micellar growth, the SLS data were analyzed by the model developed for polymer-like micelles [44] with the assumption that the actual weight-average molecular weight (M_w) of micelles increases with surfactant concentration following a power-law of the form:

$$M_w = B_1 c^a, \tag{11}$$

where B_1 is a prefactor and a is the growth exponent.

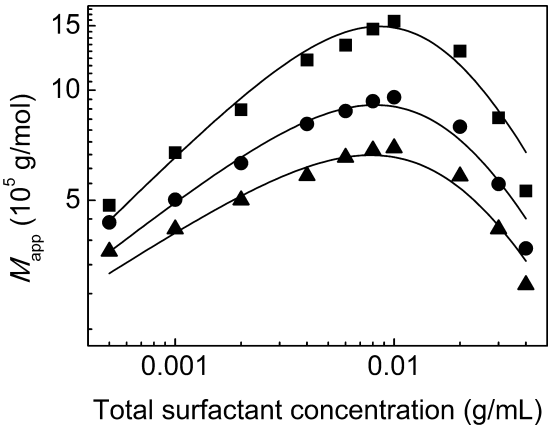

Fig. 5. Concentration dependence of the apparent molecular weight of micelles (M_{app}): (■) $\alpha = 0$, (●) $\alpha = 0.05$ and (▲) $\alpha = 0.1$. The solid lines represent the best fits of data to Eqs. (11)–(14).

In this model, the relationship between M_{app} and M_w is given by:

$$M_{app} = M_w S(0) \tag{12}$$

where $S(0)$ is the static structure factor for $q = 0$ [see Eq. (2)] and expressed as [45]:

$$S(0)^{-1} = 1 + \frac{1}{8}\left[9X - 2 + \frac{2\ \ln(1+X)}{X}\right] \exp\left\{\frac{1}{2.565}\left[\frac{1}{X} + \left(1 - \frac{1}{X^2}\right)\ln(1+X)\right]\right\}. \tag{13}$$

In Eq. (13), $X = c/c^*$ is a dimensionless concentration and given by:

$$X = 2.10 B_1^{3\nu-1} B_2 c^{[a(3\nu-1)+1]}. \tag{14}$$

Here, $\nu = 0.588$ is kept constant as the situation for micelles with excluded volume interactions corresponds to good-solvent conditions for polymers. The parameter B_2 corresponds to the second virial coefficient A_2 through $A_2 = B_2 M_w^{3\nu-2}$ [46].

Combining Eqs. (11)–(14), a quantitative description of the micellar growth was obtained and the parameters are listed in Table 2. It is obvious that the addition of TX-Ni caused a dramatic decrease of B_1. Because the prefactor B_1 is a direct measure of M_w, its reduction indicates that the micellar growth was inhibited by the addition of TX-Ni. This was attributed to the increased steric and electrostatic repulsion caused by the insertion of TX-Ni [47]. As mentioned above, the variation of B_2 is related to the second virial coefficient. Generally, a larger attractive interaction leads to a more negative A_2 [48]. The slight increase of positive B_2 suggests that water was a good solvent for the micelles and the repulsive interactions between micelles were enhanced by the insertion of TX-Ni, and therefore micelle coacervation was inhibited [49,50].

The effect of TX-Ni on micellar growth was also studied by DLS. It can be seen from Fig. 6 that the hydrodynamic diameter (D_H) of micelles decreased with the addition of TX-Ni. This is consistent with the result of SLS experiments.

Table 2
Best fit values of the growth exponent a in Eq. (11) and the parameters B_1 and B_2 in Eqs. (11) and (14) obtained using $\nu = 0.588$.

α	a	B_1 (10^7 g$^{(1-a)}$ mL^{3a} mol^{-1})	B_2 (10^{-4} mL^3 mol$^{0.764}$ g$^{-1.764}$)
0	0.60	3.0	3.2
0.05	0.47	0.9	4.2
0.10	0.39	0.4	4.8

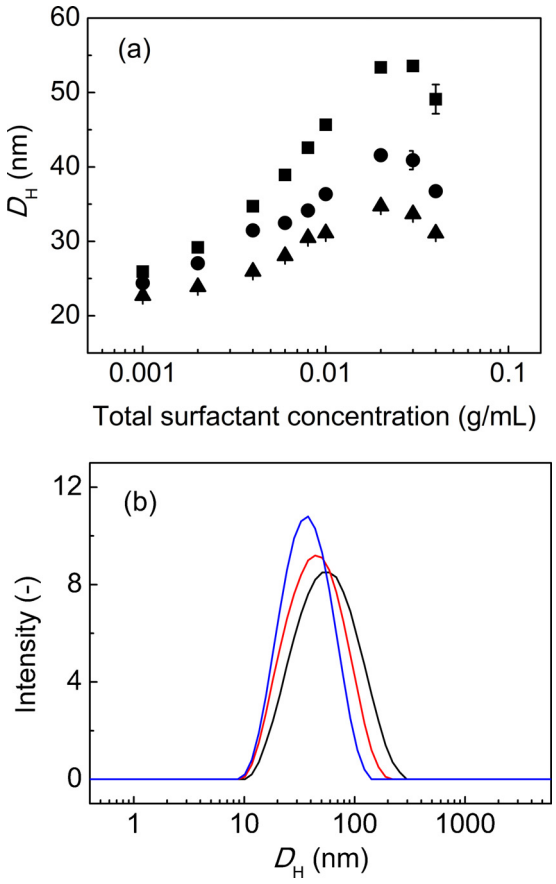

Fig. 6. (a) Concentration dependence of the hydrodynamic diameter of micelles (D_H): (■) $\alpha = 0$, (●) $\alpha = 0.05$ and (▲) $\alpha = 0.1$. (b) The intensity distribution of D_H at $\alpha = 0$ (black), 0.05 (red) and 0.1 (blue) with a total surfactant concentration of 0.01 g/mL. (For interpretation of the references to color in this figure legend, the reader is referred to the web version of this article.)

3.5. Partitioning of proteins in ATPMS

ATPMSs have been considered as attractive systems for bioseparation. However, the low specificity remains to be an obstacle that limits their application. Generally, immobilized metal-ion ligands are used for the functionalization of materials to achieve affinity separation of proteins [21,51–54].

In this work, two model proteins, EGFP (29 kDa) and lysozyme (14 kDa), were used to examine the capability of the affinity-based ATPMS for protein separation. The recombinant EGFP contains a hexahistidine tag, whereas lysozyme exposes only one histidine residue at the protein surface [55]. Therefore, they are good representatives of histidine-rich and histidine-poor proteins for investigating the metal-chelate affinity for histidine. Additionally, the target protein, EGFP, was stable in solutions containing TX. Although TX-Ni could induce significant denaturation of EGFP, no obvious influence was observed when α was no more than 0.1 as revealed by the nearly 100% mass balance (data not shown).

The experimental conditions and results are summarized in Table 3. Since the surfactant concentration after mixing lay at the mid-point of the tie-line, a 1:1 volume ratio was obtained [15]. It is interesting to see that EGFP was extracted into the micelle-rich phase with increasing TX-Ni, whereas the partitioning of lysozyme was scarcely influenced. In the ATPMS composed of only TX, the partition coefficient of EGFP was smaller than unity ($K_P = 0.60$). This result is consistent with that of Lopes et al. [56], indicating that hydrophilic EGFP preferred to partition into the micelle-poor phase where more free volume is available. However, the

Table 3
Partitioning experiments of EGFP and lysozyme in ATPMSs.

α	Temperature (°C)	EGFP			Lysozyme		
		V_R	K_P	E (%)	V_R	K_P	E (%)
0	27.56	1.02 ± 0.03	0.60 ± 0.01	36.8 ± 0.9	1.06 ± 0.05	0.84 ± 0.03	47.0 ± 0.4
0.001	27.78	1.05 ± 0.03	1.57 ± 0.06	60.4 ± 2.1	1.05 ± 0.02	0.84 ± 0.01	46.2 ± 0.1
0.005	28.10	1.00 ± 0.03	2.80 ± 0.04	70.8 ± 0.6	1.02 ± 0.01	0.86 ± 0.02	45.5 ± 1.4
0.01	28.46	1.03 ± 0.02	3.61 ± 0.07	75.3 ± 0.7	1.03 ± 0.01	0.84 ± 0.02	46.6 ± 0.9
0.02	29.42	1.02 ± 0.04	6.57 ± 0.04	83.0 ± 1.8	1.03 ± 0.03	0.85 ± 0.02	46.1 ± 0.4
0.05	31.38	1.04 ± 0.01	9.92 ± 0.19	86.5 ± 0.8	1.02 ± 0.03	0.87 ± 0.01	46.2 ± 0.8
0.1	34.63	1.03 ± 0.02	12.42 ± 0.20	87.6 ± 1.0	1.02 ± 0.01	0.86 ± 0.01	46.2 ± 1.2

Table 4
Affinity separation of EGFP and lysozyme by the affinity-based ATPMS.[a]

Protein	K_P (–)	E (%)	S (–)
EGFP	11.88 ± 0.19	83.8 ± 1.2	13.2
Lysozyme	0.90 ± 0.07	45.4 ± 1.9	–

[a] Initial conditions were surfactant solution: [TX] + [TX-Ni] = 0.08 g/mL, α = 0.1, 1.5 mL; protein solution: 0.2 mg/mL EGFP and 0.2 mg/mL lysozyme, 1.5 mL. After thorough mixing at 4 °C, the homogeneous mixture was placed at 34.63 °C for 2 h.

presence of TX-Ni changed the partitioning behavior of EGFP and an over 20-fold increase (from 0.60 to 12.42) of K_{EGFP} was obtained at α = 0.1. Because the surfactant concentration in each coexisting phase was almost the same for all cases, as it was approximately equal to the intersection of the operating tie-line and the fitted coexistence curve [15], the increase of K_{EGFP} was mainly caused by the affinity interaction between histidine residues and TX-Ni. As for lysozyme, in all cases, it was prone to partition into the micelle-poor phase due to excluded-volume interactions [13] and the extraction yields remained nearly the same. It is worth noting that, at α = 0, K_{EGFP} was smaller than K_{LYZ}. This is because the excluded-volume interaction increases with molecular weight [13]. Finally, the separation of EGFP and lysozyme was performed in the affinity-based ATPMS. As listed in Table 4, EGFP was selectively extracted to the micelle-rich phase with a separation factor of 13.2. These results demonstrated the selective separation of histidine-rich proteins from histidine-poor proteins. Considering that poly-histidine is a widely used fusion tag to facilitate protein purification [57], TX-Ni is promising to extend the application of ATPMSs.

4. Conclusions

A novel Ni(II)-chelated surfactant TX-Ni was prepared from TX by successive modifications with epichlorohydrin and IDA followed by chelating with nickel ions. Although TX is thermosensitive, no phase separation behavior was observed for the aqueous solution of TX-Ni. Therefore, TX-Ni was mixed with TX to form an affinity-based ATPMS. As TX-Ni had a more hydrophilic head group than TX, the efficient dehydration of mixed micelles took place at higher temperature, and the cloud point thus increased with the mole fraction of TX-Ni. Moreover, the insertion of TX-Ni increased the steric and electrostatic repulsion between the head groups of surfactants, and therefore the micellization process and micellar growth were inhibited. In the ATPMS formed by TX-Ni and TX, EGFP partitioned into the micelle-rich phase where it was normally excluded and an over 20-fold increase (from 0.60 to 12.42) of K_{EGFP} was obtained. The selective separation of EGFP from a mixture with lysozyme demonstrated the efficiency of TX-Ni as an affinity surfactant. The application of the Ni(II)-chelated ATPMS in protein separation remains to be further studied, but this study reveals the potential of this affinity-based ATPMS for the separation of histidine-rich proteins.

Acknowledgements

This work was supported by the Natural Science Foundation of China (Nos. 21076149 and 21236005) and the Natural Science Foundation of Tianjin from Tianjin Municipal Science and Technology Commission (Contract no. 13JCZDJC27700).

Appendix A. Supplementary data

Supplementary data associated with this article can be found, in the online version, at http://dx.doi.org/10.1016/j.chroma.2013.10.074.

References

[1] J.A. Asenjo, B.A. Andrews, J. Chromatogr. A 1218 (2011) 8826.
[2] J.A. Asenjo, B.A. Andrews, J. Chromatogr. A 1238 (2012) 1.
[3] F. Ruiz-Ruiz, J. Benavides, O. Aguilar, M. Rito-Palomares, J. Chromatogr. A 1244 (2012) 1.
[4] P.A.J. Rosa, A.M. Azevedo, S. Sommerfeld, W. Bäcker, M.R. Aires-Barros, Biotechnol. Adv. 29 (2011) 559.
[5] P.A.J. Rosa, I.F. Ferreira, A.M. Azevedo, M.R. Aires-Barros, J. Chromatogr. A 1217 (2010) 2296.
[6] P.G. Mazzola, A.M. Lopes, F.A. Hasmann, A.F. Jozala, T.C.V. Penna, P.O. Magalhaes, C.O. Rangel-Yagui, A. Pessoa, J. Chem. Technol. Biotechnol. 83 (2008) 143.
[7] D. Otzen, Biochim. Biophys. Acta, Proteins Proteomics 1814 (2011) 562.
[8] C.L. Liu, Y.J. Nikas, D. Blankschtein, Biotechnol. Bioeng. 52 (1996) 185.
[9] Z.L. Wang, Appl. Microbiol. Biotechnol. 75 (2007) 1.
[10] H. Watanabe, H. Tanaka, Talanta 25 (1978) 585.
[11] C. Bordier, J. Biol. Chem. 256 (1981) 1604.
[12] Y. Ali Sarafraz, TrAC Trends Anal. Chem. 30 (2011) 918.
[13] Y.J. Nikas, C.-L. Liu, T. Srivastava, N.L. Abbott, D. Blankschtein, Macromolecules 25 (1992) 4797.
[14] D.T. Kamei, D.I.C. Wang, D. Blankschtein, Langmuir 18 (2002) 3047.
[15] H. Lam, M. Kavoosi, C.A. Haynes, D.I.C. Wang, D. Blankschtein, Biotechnol. Bioeng. 89 (2005) 381.
[16] P.G. Mazzola, H. Lam, M. Kavoosi, C.A. Haynes, A. Pessoa, T.C.V. Penna, D.I.C. Wang, D. Blankschtein, Biotechnol. Bioeng. 93 (2006) 998.
[17] S. Fernandes, R. Hatti-Kaul, B. Mattiasson, Biotechnol. Bioeng. 79 (2002) 472.
[18] N. Garg, I. Galaev, B. Mattiasson, Biotechnol. Appl. Biochem. 20 (1994) 199.
[19] T. Saitoh, W.L. Hinze, Talanta 42 (1995) 119.
[20] A.M. Lopes, A. Pessoa, C.D. Rangel-Yagui, Quim. Nova 31 (2008) 998.
[21] J. Lu, D.-Q. Lin, S.-J. Yao, Ind. Eng. Chem. Res. 45 (2006) 1774.
[22] U. Sivars, J. Abramson, S. Iwata, F. Tjerneld, J. Chromatogr. B 743 (2000) 307.
[23] X.-Y. Dong, X.-D. Feng, Y. Sun, Biotechnol. Prog. 26 (2010) 1088.
[24] X.-Y. Dong, Y. Meng, X.-D. Feng, Y. Sun, Biotechnol. Prog. 26 (2010) 150.
[25] R. Cheung, J. Wong, T. Ng, Appl. Microbiol. Biotechnol. 96 (2012) 1411.
[26] X.-Y. Dong, L.-J. Chen, Y. Sun, J. Chromatogr. A 1216 (2009) 5207.
[27] H.-C. Kang, B. Lee, J. Yoon, M. Yoon, J. Am. Oil Chem. Soc. 78 (2001) 423.
[28] A. Aserin, N. Garti, Y. Sasson, Ind. Eng. Chem. Prod. Res. Dev. 23 (1984) 452.
[29] T. Takasu, A. Iles, K. Hasebe, Anal. Bioanal. Chem. 372 (2002) 554.
[30] J. Aguiar, P. Carpena, J.A. Molina-Bolı́var, C.C. Ruiz, J. Colloid Interface Sci. 258 (2003) 116.
[31] B.H. Zimm, J. Chem. Phys. 16 (1948) 1093.
[32] M. Liley, T.A. Keller, C. Duschl, H. Vogel, Langmuir 13 (1997) 4190.
[33] P. Mukherjee, S.K. Padhan, S. Dash, S. Patel, B.K. Mishra, Adv. Colloid Interface Sci. 162 (2011) 59.
[34] S.B. Sulthana, P.V.C. Rao, S.G.T. Bhat, T.Y. Nakano, G. Sugihara, A.K. Rakshit, Langmuir 16 (2000) 980.
[35] T. Gu, P.A. Galera-Gómez, Colloids Surf. A 104 (1995) 307.
[36] V.C. Santos, F.A. Hasmann, A. Converti, A. Pessoa Jr., Biochem. Eng. J. 56 (2011) 75.
[37] A. Sánchez-Ferrer, M. Pérez-Gilabert, E. Núñez, R. Bru, F. García-Carmona, J. Chromatogr. A 668 (1994) 75.
[38] P.M. Holland, D.N. Rubingh, J. Phys. Chem. 87 (1983) 1984.

[39] M.E. Haque, A.R. Das, A.K. Rakshit, S.P. Moulik, Langmuir 12 (1996) 4084.
[40] S.R. Patil, N. Buchavzov, E. Carey, C. Stubenrauch, Soft Matter 4 (2008) 840.
[41] X. Li, S. Dong, J. Hao, Soft Matter 5 (2009) 990.
[42] M. Bergström, J.C. Eriksson, Langmuir 16 (2000) 7173.
[43] I. Grillo, J. Penfold, Langmuir 27 (2011) 7453.
[44] P. Schurtenberger, C. Cavaco, F. Tiberg, O. Regev, Langmuir 12 (1996) 2894.
[45] P. Bäverbäck, C.L.P. Oliveira, V.M. Garamus, I. Varga, P.M. Claesson, J.S. Pedersen, Langmuir 25 (2009) 7296.
[46] U. Menge, P. Lang, G.H. Findenegg, J. Phys. Chem. B 103 (1999) 5768.
[47] A. Shiloach, D. Blankschtein, Langmuir 14 (1998) 7166.
[48] S. Brunetti, D. Roux, A.M. Bellocq, G. Fourche, P. Bothorel, J. Phys. Chem. 87 (1983) 1028.
[49] L. Yang, X. Qi, P. Liu, A. El Ghzaoui, S. Li, Int. J. Pharm. 394 (2010) 43.
[50] C. Ruiz, J. Molina-Bolívar, J. Hierrezuelo, E. Liger, Int. J. Mol. Sci. 14 (2013) 3228.
[51] N.S. Bibi, N.K. Singh, R.N. Dsouza, M. Aasim, M. Fernández-Lahore, J. Chromatogr. A 1272 (2013) 145.
[52] M. Erzengin, N. Ünlü, M. Odabaşı, J. Chromatogr. A 1218 (2011) 484.
[53] L. Novotna, T. Emmerova, D. Horak, Z. Kucerova, M. Ticha, J. Chromatogr. A 1217 (2010) 8032.
[54] R.R. Prasanna, M.A. Vijayalakshmi, J. Chromatogr. A 1217 (2010) 3660.
[55] F.B. Anspach, J. Chromatogr. A 676 (1994) 249.
[56] A.M. Lopes, P.O. Magalhães, P.G. Mazzola, C.O. Rangel-Yagui, J.C.M. de Carvalho, T.C.V. Penna, A. Pessoa Jr., Sep. Purif. Technol. 81 (2011) 339.
[57] K. Terpe, Appl. Microbiol. Biotechnol. 60 (2003) 523.